Hindawi
Journal of Chemistry
Volume 2019, Article ID 1743147, 14 pages
https://doi.org/10.1155/2019/1743147

Research Article

Synthesis, Characterization, and Biological Evaluation of a New Hydrogen-Bonded Charge-Transfer Complex of 2-Amino-4-methoxy-6-methylpyrimidine

Reem M. Alghanmi

Department of Chemistry, Faculty of Science, University of Jeddah, Jeddah 80327/21589, Saudi Arabia

Correspondence should be addressed to Reem M. Alghanmi; rmalghanmi2018@gmail.com

Received 18 May 2019; Revised 22 November 2019; Accepted 26 November 2019; Published 16 December 2019

Academic Editor: Franck Rabilloud

A new hydrogen-bonded charge-transfer (HB-CT) complex formed between the donor 2-amino-4-methoxy-6-methylpyrimidine (AMMP) and the π-acceptor 2,5-dihydroxy-*p*-benzoquinone (DHBQ) was investigated in both solid and solution states. The investigation was conducted using UV-Vis, CHN, FTIR, ^{1}H NMR, XRD, and TG-DTA analyses. The molecular composition of the CT complex in MeOH was found to be 1 : 1. The formation constant (K_{CT}), molecular extinction coefficient (ε), and several other spectroscopic physical parameters were evaluated at different temperatures. The thermodynamic properties of the CT interaction in MeOH were studied by calculating the enthalpy (ΔH°), entropy (ΔS°), and free energy (ΔG°). The thermodynamic parameters indicated that van der Waals interactions and hydrogen bonding occur between AMMP and DHBQ in MeOH. The CHN, FTIR, and TG-DTA measurements confirmed that the solid HB-CT complex forms in a 2 : 1 ratio, i.e., $[(AMMP)_2(DHBQ)]$, and exhibits high stability. Moreover, XRD analysis was used to establish that the mean particle size of the complex is 23 nm. Finally, the solid HB-CT complex was screened for its antibacterial, antifungal, and antioxidant activities. It shows good activity against various bacterial and fungal species. Furthermore, the HB-CT complex exhibits good DPPH scavenging activity.

1. Introduction

The synthesis and characterization of new hydrogen-bonded charge-transfer (HB-CT) complexes that have biological activities have attracted significant research interest in recent years [1–3]. This interest is largely due to the significant role that HB-CT complexes play in biological systems as antibacterial and antifungal compounds as well as the DNA binding these complexes exhibit [4–6]. Furthermore, CT complexes are widely applied in surface chemistry [7], solar energy storage systems [8], organic superconductors [9], and optical devices [10]. Moreover, the HB-CT interactions of many heterocyclic drugs with various π-acceptors have been exploited in pharmaceutical analysis [11–13] and to further our understanding of drug-receptor mechanisms [14].

Aminopyrimidines are very important *N*-heterocyclic compounds that have numerous pharmaceutical applications and biological activities [15–17]. They are present in both natural and synthetic products [18]. Moreover, some aminopyrimidine derivatives have been explored as antithrombus, antimicrobial, antifungal, and anti-HIV agents [19–21]. They also form a range of organometallic complexes with anticancer and antioxidant activities [22–24]. Aminopyrimidines contain important groups that can act as electron donors or proton acceptors, and the study of their CT complexes helps to understand the nature of their CT interactions [25, 26].

Previous studies on HB-CT complexes [27–30] and the well-documented biological importance of aminopyrimidines prompted us to investigate the ability of the simple pyrimidine derivative 2-amino-4-methoxy-6-methylpyrimidine (AMMP) as an electron donor in an HB-CT complex with the electron acceptor 2,5-dihydroxy-*p*-benzoquinone (DHBQ) in both solid and solution states (Scheme 1). The reaction stoichiometry, HB-CT properties, and thermal stability of the complex in MeOH have been

estimated using UV-Vis spectrometry, whereas the solid HB-CT complex was characterized using FTIR spectroscopy, ^{1}H NMR, powder XRD, and TG/DTA. The antifungal and antibacterial activities of the HB-CT complex were explored, and the antioxidant activity of the new HB-CT complex against DPPH radicals was evaluated.

2. Materials and Methods

All chemicals used, including AMMP (Acros Organics, 98%) and DHBQ (Aldrich Chemicals, 98%), were of analytical grade. The MeOH was of spectroscopic grade and was used without further purification. Standard solutions of AMMP (1×10^{-2} mol L^{-1}) and DHBQ (5×10^{-3} mol L^{-1}) were prepared in MeOH before each measurement. The standard solutions of AMMP and DHBQ were kept in a cold and dark place for at least one week prior to use. The HB-CT solutions for UV-Vis spectroscopic measurements were prepared by mixing appropriate aliquots of AMMP and DHBQ standard solutions and then diluted with MeOH.

The electronic absorption spectra of all solutions were recorded in the region from 700 to 300 nm with a UV-Vis spectrophotometer (Shimadzu UV-1800, Japan), which was connected to a temperature controller unit (Shimadzu TCC-ZUOA). The CHN contents were measured with a micro-analyzer (PerkinElmer 2400, USA). The FTIR spectra of the AMMP, DHBQ, and their solid HB-CT complex were measured as KBr discs using a Frontier spectrometer (PerkinElmer, USA). ^{1}H NMR (600 MHz) spectra were recorded on a Bruker DPX spectrometer using 10 mg of the sample in DMSO-d_6 and TMS as an internal standard. Thermal analyses were performed using a Pyris 6 TGA apparatus (PerkinElmer, USA). Powder XRD patterns were obtained on a Model Equinox1000 diffractometer (INEL, France) with Co K_α ($\lambda = 1.7890$ Å) radiation at 30 kV and 30 mA. Minimal sample preparation was required for analysis; the sample was simply packed into a sample holder and placed in the instrument. The powdered sample was scanned over a 2θ range from 0° to 120°.

2.1. Synthesis of the Solid CT Complex. The solid HB-CT complex was prepared by dissolving equimolar amounts (0.5 mmol) of AMMP and DHBQ in MeOH (25 mL). The AMMP solution was added to the DHBQ solution, and the mixture was stirred for 30 min. Then, the solvent was allowed to evaporate at room temperature. The HB-CT complex was obtained as a dark-pink solid product, which was filtered and washed with MeOH. The CHN contents and physical data of the solid complex are given in Table 1, where the analytical calculations confirmed that the HB-CT complex was formed as [(AMMP)$_2$(DHBQ)].

2.2. Antimicrobial Activity

2.2.1. Antibacterial Activity. Three Gram-positive bacteria were utilized, i.e., *Bacillus subtilis* (NRRL-B-4219), *Sarcina lutea* (ATCC 27853), and *Staphylococcus aureus* (ATCC 25923), as well as the Gram-negative microorganisms *Escherichia coli* (ATCC 25922), *Pseudomonas aeruginosa* (NRRL B23 27853), and *Klebsiella pneumoniae* (ATCC 27736). The antibacterial tests were performed by the well diffusion method [31] to compare the antibacterial activities of AMMP and the new HB-CT complex against the human pathogenic bacteria. Neomycin was utilized as per usual guidelines at 30 μg·mL^{-1}. The bacterial suspensions were balanced with saline to a convergence of 10^5 CFU·mL^{-1}. The inoculum was refined in a nutrient medium to confirm the absence of tainting and to check the utility of the inoculum. Colonies were spread onto plates, and wells were made utilizing a cork borer (8 mm). Wells were loaded with 10 μg·mL^{-1} of engineered mixes diluted with dimethyl sulfoxide (DMSO). The Petri dishes were kept aseptically for 4 to 5 h. Then, all the Petri dishes were incubated for 24 h at 32°C, and the development inhibition zones were estimated.

2.2.2. Antifungal Activity. Potato dextrose agar medium was used to investigate the antifungal activities of AMMP and the new HB-CT complex. The medium was sterilized in an autoclave for 15 min at 15 psi. Then, it was transferred aseptically into Petri plates. The contagious strains, yeasts, such as *Candida albicans* (ATCC 10231), *Aspergillus niger* (NRRL-3), and *Penicillium* sp. were inoculated on the surface of the Petri plates independently after two hours. The parasitic suspensions were balanced with clean saline to 10^4 spores·mL^{-1} [32, 33]. The inoculums were refined in a strong medium to confirm the absence of tainting and to check the utility of the inoculum. Colonies were spread onto the plates, and then wells were made utilizing a cork borer (8 mm). Wells were loaded with complex diluted with DMSO to 50 μg·mL^{-1}. These Petri plates were incubated for 48 h at a temperature of 28 ± 2°C, and then the development of inhibition zones (in mm) was assessed. The zone of inhibition (mm) for each compound was compared with that of a tetracycline standard. Finally, the best outcomes were repeated at a compound concentration of 30 μg·mL^{-1}.

2.3. ADPPH Radical Scavenging Activity. The antioxidant activity of ethanolic AMMP and the HB-CT complex was assessed in terms of DPPH radical scavenging ability [34]. The optical densities of samples without DPPH were subtracted from those with DPPH to eliminate the background. The decrease (%) values were compared with ascorbic acid (Asa) as a standard. The inhibition of DPPH was calculated as a percentage (I%).

3. Results and Discussion

3.1. Electronic Absorption Spectra and Molecular Composition. The electronic absorption spectra of the AMMP, DHBQ, and their mixture in MeOH were recorded in the range of 700–300 nm, as shown in Figure 1. An absorption band centered at 488 nm is observed in the visible region of the mixture that is not present in the free AMMP and DHBQ absorption spectra. Moreover, the appearance of this band is accompanied by a change in the mixture color,

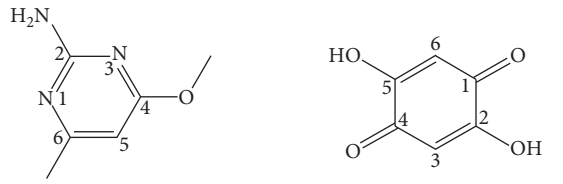

2-Amino-4-methoxy-6-methylpyrimidine (AMMP)

2,5-Dihydroxybenzoquinone (DHBQ)

Scheme 1: Chemical structures of AMMP and DHBQ.

where an orange solution was obtained as shown in Figure 2. The suggested mechanism for the formation of this CT complex in a polar solvent such as MeOH involves the formation of an initial outer sphere CT complex followed by the complete transfer of electrons from the AMMP to the DHBQ, leading to the formation of intensely colored radical ions, as shown in Scheme 2 [27, 28]. All complex spectra were recorded against DHBQ solution as a blank [27, 28].

The molecular composition of the formed complex was determined by using Job's method of continuous variation [35]. Equimolar concentrations (5×10^{-3} mol·L^{-1}) of both AMMP and DHBQ in MeOH were used. A series of mixtures of AMMP and DHBQ was prepared in which the total volume was kept at 4 mL. The AMMP and DHBQ were mixed in different ratios (0.5 : 3.5; 1.0 : 3.0; . . .; 3.5 : 0.5) and then complete the volume to 10 mL with solvent (MeOH). The absorbance of the formed complex was measured at 488 nm against the DHBQ solution as blank. The maximum absorbance was recorded at 0.5 mol fraction, indicating the formation of 1 : 1 complex (AMMP : DHBQ) (Figure 3). Also, the 1 : 1 molecular composition was confirmed by using the photometric and conductometric titrations [29] (Figures 4 and 5).

3.2. Determination of Formation Constant and Spectroscopic Physical Parameters. The electronic absorption spectra of the CT complex were recorded with increasing AMMP concentration from 2.0×10^{-4} mol·L^{-1} to 10×10^{-4} mol· L^{-1} and a fixed DHBQ concentration (5×10^{-4} mol·L^{-1}). The CT solutions were analyzed at different temperatures (20°C, 25°C, 30°C, 35°C, and 40°C). Figure 6 shows the electronic spectra of the CT complex at different temperatures, demonstrating that the absorbance decreases with increasing temperature. Moreover, the CT complex band was found to be stable for more than 2 h at room temperature (20°C). The absorbance values of the CT complex at λ_{max} for different concentrations of AMMP and at different temperatures are shown in Table 2. The values of the formation constant (K_{CT}) and the molar absorptivity (ε) at different temperatures were calculated by applying the modified Benesi–Hildebrand equation [36] for 1 : 1 stoichiometry as follows:

$$\frac{C_D^o C_A^o}{\text{Abs}} = \frac{1}{K_{CT}\varepsilon} + \frac{\left(C_D^o + C_A^o\right)}{\varepsilon}, \quad (1)$$

where C_D^o and C_A^o are the concentrations of the donor (AMMP) and acceptor (DHBQ), respectively, and Abs is the absorbance of the CT complex at a given concentration. Plotting $C_D^o C_A^o$/Abs versus $(C_D^o + C_A^o)$ for the formed CT complex at different temperatures produces straight lines, indicating the formation of a 1 : 1 complex (Figure 7). The concentrations of donor and acceptor, which were used in BH plots, are presented in Table 2. The values of K_{CT} and ε were calculated from the slopes and intercepts of the lines at different temperatures, and the results are given in Table 2.

The values of K_{CT} and ε are high, which confirms the high stability of the formed CT complex in MeOH. Also, the high values of both K_{CT} and ε indicate the strong interaction between AMMP and DHBQ and the presence of hydrogen bonds in the complex formed. The high stability of the HB-CT complex may also be due to MeOH acting as both a hydrogen bond donor and a hydrogen bond acceptor. Based on Kamlet–Taft solvent parameters [37], MeOH has high values of both hydrogen bond donating ability (α, 0.98) and hydrogen bond accepting ability (β, 0.62). Therefore, MeOH can form hydrogen bonds as H-donor with the basic centers in AMMP and in DHBQ, as well as with the primary amine protons of AMMP and the protons of the OH groups of DHBQ as an H-acceptor. Thus, these bonds are assumed to increase the stability of the formed HB-CT complex [38].

From the spectral data of the HB-CT complex in MeOH, several spectroscopic physical parameters were calculated and evaluated. The ionization potential (I_D) of the free donor (AMMP) in the HB-CT complex was calculated by applying the equation derived by Aloisi and Pignataro [39]:

$$I_D = 5.76 + 1.53 \times 10^{-4} \cdot \nu_{CT}, \quad (2)$$

where ν_{CT} is the wavenumber in cm^{-1} of the HB-CT band. The value of the AMMP ionization potential in MeOH is given in Table 3, and it is a relatively low value, which indicates the good donating power of AMMP and thus the high stability of the formed HB-CT complex.

The experimental oscillator strength (f) [40] and the transition dipole moment (μ) [41] of the HB-CT complex were calculated at different temperatures using the following equations [42]:

$$f = \left(4.32 \times 10^{-9}\right) \cdot \varepsilon_{CT} \cdot \Delta\nu_{1/2},$$
$$\mu = 0.0958 \cdot \sqrt{\frac{\varepsilon_{CT} \cdot \Delta\nu_{1/2}}{\nu_{CT}}}, \quad (3)$$

where $\Delta\nu_{1/2}$ is the half bandwidth in cm^{-1} of the HB-CT band, and ε_{CT} and ν_{CT} are the molar extinction coefficient and wavenumber of the CT band, respectively. The values of both f and μ are given in Table 3. The high values of both f and μ indicate the strong HB-CT interaction between AMMP and DHBQ in MeOH.

An important finding from Table 3 is that the values of both f and μ decrease with increasing temperature, which indicates that the stability of the HB-CT complex decreases with increasing temperature. These results can also be confirmed by the decreased in K_{CT} values with increasing temperature as shown in Table 2.

Table 1: CHN contents and physical data of the solid HB-CT complex.

Complex	MW (g·mol^{-1})	C (%)		H (%)		N (%)		Physical data	
		Found	Calc.	Found	Calc.	Found	Calc.	Color	mp (°C)
[(AMMP)$_2$(DHBQ)]	418.41	47.11	47.25	3.61	3.94	12.18	12.25	Dark pink	240

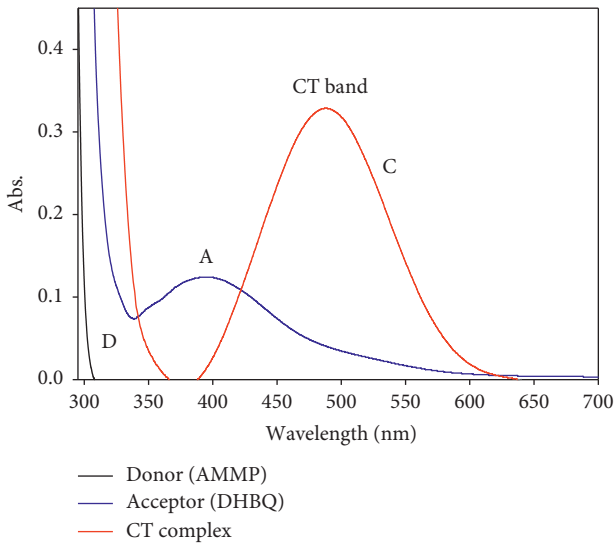

Figure 1: Electronic spectra: (D) 1×10^{-3} mol·L^{-1} (AMMP), (A) 5×10^{-4} mol·L^{-1} (DHBQ), and (C) [1×10^{-3} mol·L^{-1} (AMMP) + 5×10^{-4} mol·L^{-1} (DHBQ)], in MeOH.

The high values of K_{CT}, f, and μ are consistent with the low CT energy value (E_{CT}) calculated using the following equation [43]:

$$E_{CT} = \frac{1243667}{\lambda_{CT}}. \quad (4)$$

Finally, the resonance energy (R_N) of the HB-CT complex in the ground state was determined by applying the following relationship derived by Briegleb and Czekalla [44], and the result is given in Table 3:

$$\varepsilon_{CT} = \frac{7.7\times10^4}{[h\nu_{CT}/[R_N] - 3.5]}. \quad (5)$$

The R_N value of the CT complex is high in MeOH, which suggests that the complex is strongly bound in this solvent and exhibits good resonance stabilization [45].

3.3. Determination of Thermodynamic Parameters. The thermodynamic parameters ΔH° and ΔS° were calculated based on the values of K_{CT} at various temperatures by applying the van't Hoff relationship [46]:

$$\ln K_{CT} = \frac{\Delta H^\circ}{RT} + \frac{\Delta S^\circ}{R}, \quad (6)$$

where ΔH° and ΔS° are the enthalpy and entropy changes during the charge-transfer process. A straight line was obtained by plotting ln K_{CT} against $1000/T$, as shown in Figure 8. The slope and the intercept of the line represent the values of ΔH° and ΔS°. The values of K_{CT} at different temperatures and the ΔH° and ΔS° values are given in Table 4.

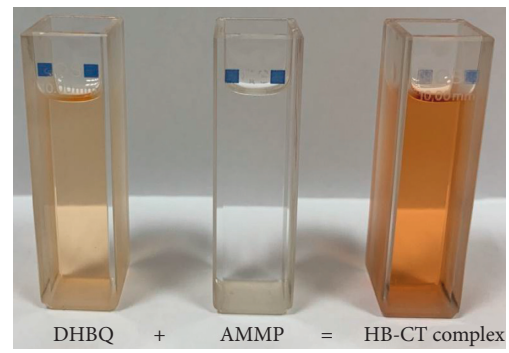

Figure 2: Naked-eye visible color change in the solution when adding DHBQ (5×10^{-4} mol·L^{-1}) to AMMP (1×10^{-3} mol·L^{-1}).

From Table 4, it is apparent that the HB-CT complex is less stable when the temperature is higher. Moreover, the enthalpy of the charge-transfer reaction is high and negative, indicating that the reaction is an exothermic process. It has been reported that, when the values of ΔH° and ΔS° are negative, van der Waals interactions and hydrogen bonding take place [47]. Thus, van der Waal interactions or hydrogen bonds are the main forces between AMMP and DHBQ in the formed HB-CT complex.

The standard free energy change of the charge-transfer interaction (ΔG°) was determined from the K_{CT} values at different temperatures by applying the following equation [48]:

$$\Delta G^\circ = -2.303RT \log K_{CT}, \quad (7)$$

where ΔG° is the free energy change of the complex (kJ mol^{-1}), R is the gas constant (8.314 mol^{-1} K), T is the absolute temperature, and K_{CT} is the formation constant of the HB-CT complex (L mol^{-1}). Table 4 gives the calculated values of ΔG° at different temperatures. The values of ΔG° are negative, which confirms the spontaneous formation of the [AMMP-DHBQ] HB-CT complex. Furthermore, it is clear from Table 4 that the values of ΔG° become more negative as K_{CT} increases because when the CT bonding becomes stronger, the components are subjected to more physical strain and less freedom; thus, the values of ΔG° became more negative [49].

3.4. Quantification Parameters. To determine the limit of detection for the HB-CT complex, different aliquots (0.1, 0.25, 0.5, ..., 5.0 mL) of a standard solution of AMMP (200 μg·mL^{-1}) was transferred into a series of 10 mL volumetric flasks. To each flask, 1 mL of 5×10^{-4} mol·L^{-1} DHBQ was added, and the mixture was diluted to the mark with

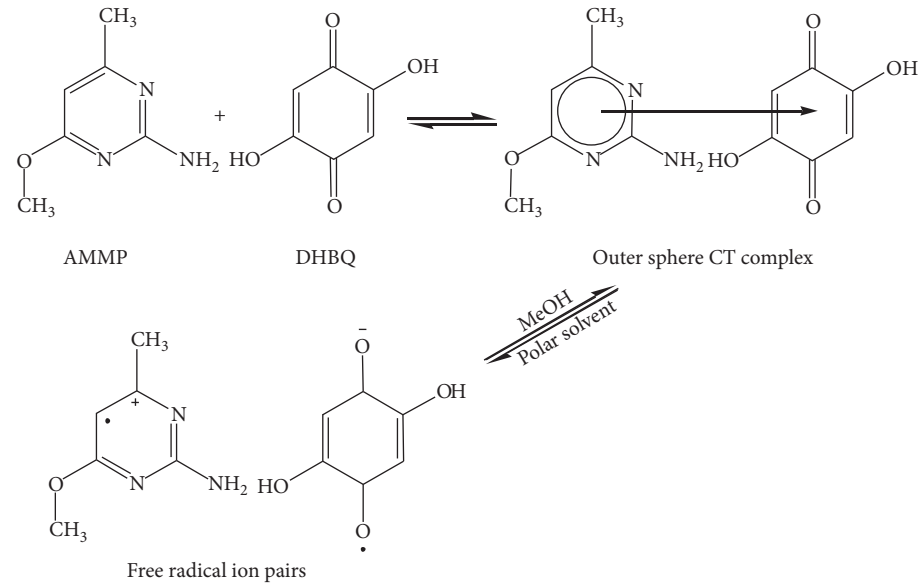

Scheme 2: The suggested mechanism for the formation of the [AMMP-DHBQ] complex in MeOH.

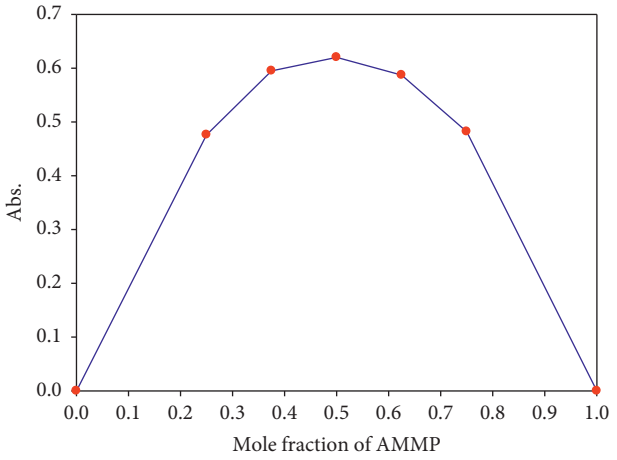

Figure 3: Job's method plot of the [AMMP-DHBQ] complex in MeOH.

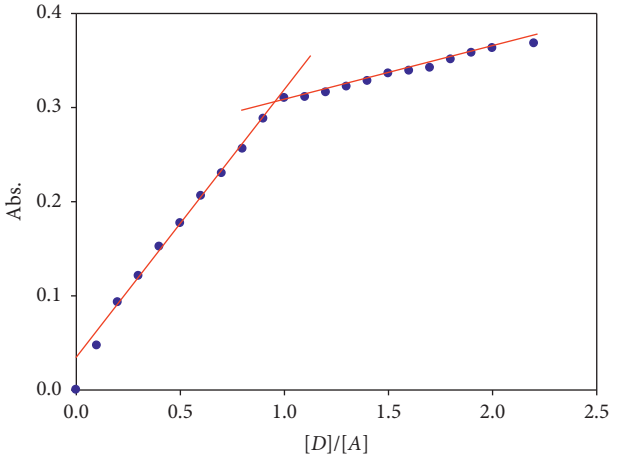

Figure 4: Photometric titration plot of the [AMMP-DHBQ] complex in MeOH.

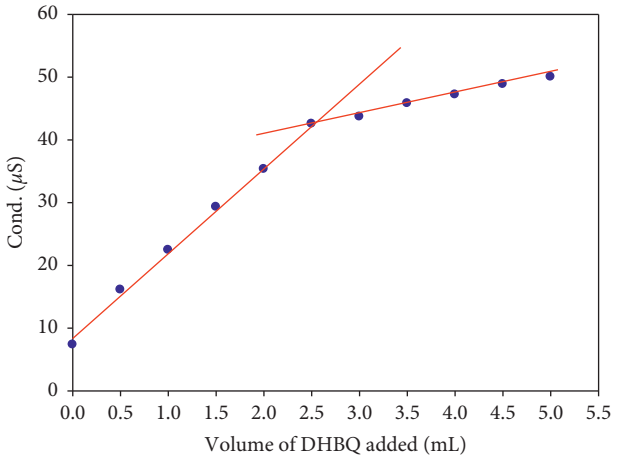

Figure 5: Conductometric titration plot of the [AMMP-DHBQ] complex in MeOH.

MeOH. The absorbance of all solutions was measured at λ_{max} (488 nm) against DHBQ blank. A standard calibration curve was constructed by plotting the absorbance of the solutions versus AMMP concentration. The regression equation of the curve was evaluated by the least-squares method [50]. The curve was linear over the concentration range of 2.00–80.0 $\mu g \cdot mL^{-1}$ AMMP with very small intercept and slope and excellent correlation coefficient (Table 5). The limit of detection (LOD) and limit of quantification (LOQ) were calculated according to the IUPAC definitions [51]:

$$\text{LOD} = \frac{3.3S_a}{b}, \qquad \text{LOQ} = \frac{10S_a}{b}, \tag{8}$$

where S_a is the standard deviation of the intercept and b is the slope of the curve. The calculated values of LOD and

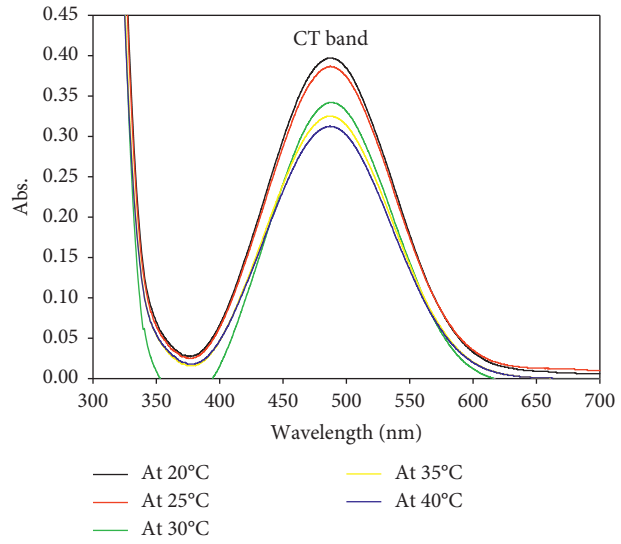

Figure 6: Electronic spectra of 8×10^{-4} mol·L^{-1} AMMP with 5×10^{-4} mol·L^{-1} DHBQ in MeOH at different temperatures.

Table 2: The absorption data, absorption maxima (λ_{CT}), formation constant (K_{CT}), and molar absorptivity (ε) of the [AMMP-DHBQ] complex in MeOH at different temperatures.

Concentration of donor AMMP (mol L^{-1})	Concentration of acceptor DHBQ (mol L^{-1})	Absorbance at λ_{CT} (nm)	Formation constant (K_{CT}) (L mol^{-1})	Molar absorptivity (ε_{CT}) (L cm^{-1} mol^{-1})	Correlation coefficient* (R^2)
At 20°C		At 488 nm	14.19×10^3	1.428×10^3	0.9955
2.0×10^{-4}	5.0×10^{-4}	0.182			
4.0×10^{-4}	5.0×10^{-4}	0.274			
6.0×10^{-4}	5.0×10^{-4}	0.341			
8.0×10^{-4}	5.0×10^{-4}	0.393			
10×10^{-4}	5.0×10^{-4}	0.436			
At 25°C		At 488 nm	9.333×10^3	1.428×10^3	0.9912
2.0×10^{-4}	5.0×10^{-4}	0.176			
4.0×10^{-4}	5.0×10^{-4}	0.266			
6.0×10^{-4}	5.0×10^{-4}	0.331			
8.0×10^{-4}	5.0×10^{-4}	0.381			
10×10^{-4}	5.0×10^{-4}	0.432			
At 30°C		At 488 nm	8.889×10^3	1.250×10^3	0.9784
2.0×10^{-4}	5.0×10^{-4}	0.166			
4.0×10^{-4}	5.0×10^{-4}	0.250			
6.0×10^{-4}	5.0×10^{-4}	0.316			
8.0×10^{-4}	5.0×10^{-4}	0.361			
10×10^{-4}	5.0×10^{-4}	0.424			
At 35°C		At 488 nm	6.229×10^3	1.250×10^3	0.9787
2.0×10^{-4}	5.0×10^{-4}	0.150			
4.0×10^{-4}	5.0×10^{-4}	0.240			
6.0×10^{-4}	5.0×10^{-4}	0.302			
8.0×10^{-4}	5.0×10^{-4}	0.347			
10×10^{-4}	5.0×10^{-4}	0.388			
At 40°C		At 488 nm	5.228×10^3	1.250×10^3	0.9964
2.0×10^{-4}	5.0×10^{-4}	0.137			
4.0×10^{-4}	5.0×10^{-4}	0.220			
6.0×10^{-4}	5.0×10^{-4}	0.272			
8.0×10^{-4}	5.0×10^{-4}	0.325			
10×10^{-4}	5.0×10^{-4}	0.355			

*The correlation coefficient of the BH plot.

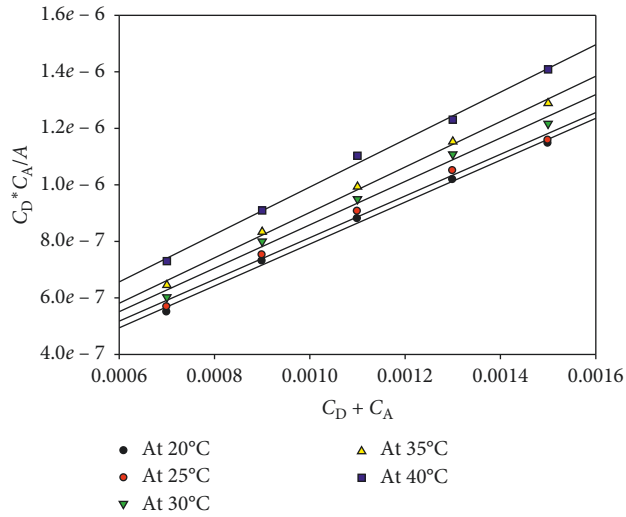

Figure 7: Benesi–Hildebrand plots of the [AMMP-DHBQ] complex in MeOH at different temperatures.

Table 3: Experimental spectroscopic physical parameters of the [AMMP-DHBQ] complex in MeOH.

Temperature (°C)	λ_{CT} (nm)	I_P (eV)	E_{CT} (eV)	$R_N \times 10^2$ (eV)	f	μ (Debye)
20		8.895		1.501	0.364	6.140
25		8.896		1.404	0.346	5.983
30	488	8.896	2.548	1.337	0.329	5.835
35		8.902		1.265	0.322	5.775
40		8.902		1.159	0.313	5.690

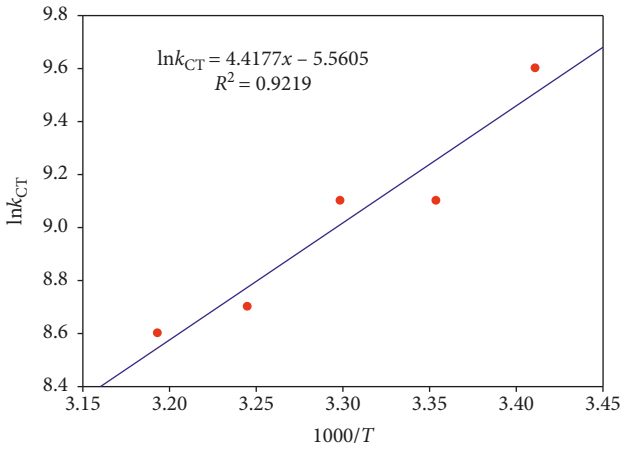

Figure 8: van't Hoff plot of the [AMMP-DHBQ] complex in MeOH.

Table 4: Formation constant at different temperatures and the thermodynamics parameters of the [AMMP-DHBQ] complex in MeOH.

Temperature (°C)	$K_{CT} \times 10^{-3}$ (L mol^{-1})	$-\Delta G^\circ$ (kJ mol^{-1})	$-\Delta H^\circ$ (kJ mol^{-1})	$-\Delta S^\circ$ (J K^{-1} mol^{-1})
20	14.19	23.69		
25	9.333	22.65		
30	8.889	22.53	36.73	46.23
35	6.229	21.65		
40	5.228	21.22		

Table 5: Quantification parameters of the HB-CT complex.

Parameter	[AMMP-DHBQ]
Beer's law limits, $\mu g{\cdot}mL^{-1}$	2.00 – 80.0
Limit of detection (LOD), $\mu g{\cdot}mL^{-1}$	0.90
Limit of quantification (LOQ), $\mu g{\cdot}mL^{-1}$	2.73
Regression equation*	$y = 0.0029x + 0.1078$
Intercept, $a \pm S_a$	$0.0029 \pm 7.84 \times 10^{-4}$
Slope, $b \pm S_b$	$0.1078 \pm 1.86 \times 10^{-5}$
Correlation coefficient, R^2	0.9996

LOQ are listed in Table 5, where they recorded small values confirming the high sensitivity of the CT reaction to detect the AMMP in low concentration using DHBQ as a reagent.

3.5. Characterization of the Solid CT Complex

3.5.1. FTIR Spectra. The FTIR spectra of the donor AMMP, acceptor DHBQ, and the solid HB-CT complex recorded as KBr disks are given in Figure 9, respectively. In the complex spectrum, the main infrared bands of the donor and acceptor are blue- or red-shifted compared with those of the isolated acceptor or donor. There is also a decrease or increase in band intensities for the complex spectrum compared with the acceptor or donor spectra as a result of the charge redistribution upon complex formation, confirming CT complex formation between DHBQ and AMMP.

A significant feature from the HB-CT complex spectrum is the change in the stretching vibration region at 3500–2500 cm^{-1}. The sharp asymmetric and symmetric stretching vibration bands for the amino and methyl groups at 3365, 3313, and 3179 cm^{-1} in the donor spectrum disappear in the complex spectrum (Figure 9). Instead, broadband is observed at 2990 cm^{-1}, which is attributed to hydrogen bond formation between the two amino groups of two donor molecules with the two hydroxyl groups of one DHBQ molecule leading to the diminution of the amino and methyl vibrational bands. Another broadband is observed at 2578 cm^{-1}, which confirms the involvement of both the amino group and one of the ring nitrogen of the AMMP in hydrogen bonding ($N^+ - H\cdots O^-$) with the hydroxyl group of the DHBQ (Scheme 3). Another important observation from the complex spectrum is the blue shifting of ν(C=O) and $\delta(NH_2)$ in the complex spectrum to 1664 cm^{-1} (doublet) compared with 1610 cm^{-1} for DHBQ alone and AMMP alone.

Furthermore, the out-of-plane deformation Υ(C=O) is observed at 660 cm^{-1} compared with 619 cm^{-1} for DHBQ alone. This confirms the formation of a 2 : 1 complex between AMMP and DHBQ through a strong donation by two donors with one strongly accepting molecule. Another important observation is the appearance of a broad absorption extending from 1400 to 400 cm^{-1} with the protonic center of gravity at 855 cm^{-1} due to the strong hydrogen bonding in the formed complex. Consequently, the formed complex exhibits high stability through charge and hydrogen bond interactions, and these results are in full agreement with the high stability constant of the complex.

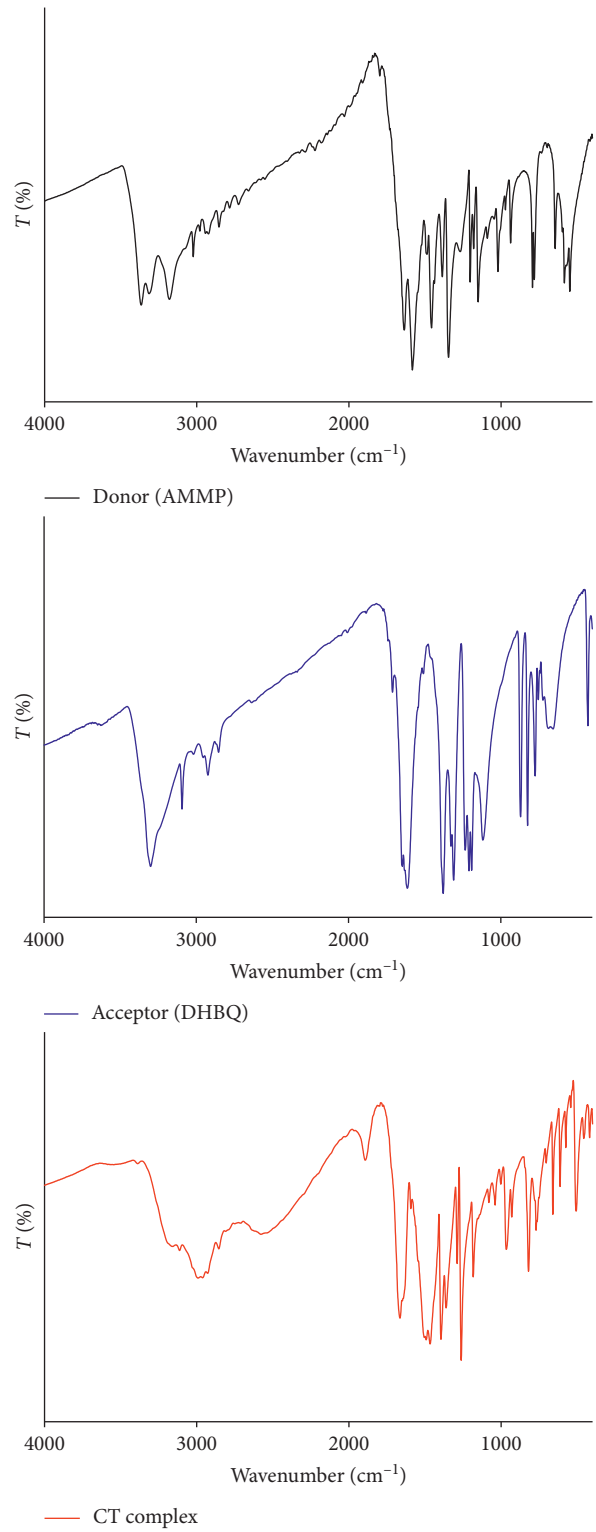

Figure 9: FTIR spectra of donor (AMMP), acceptor (DHBQ), and solid [$(AMMP)_2$(DHBQ)] complex in the range of 4000 to 400 cm^{-1}.

3.5.2. ^1H NMR Spectra. The ^1H NMR spectrum of the [$(AMMP)_2$(DHBQ)] complex in DMSO-d_6 is shown in Figure 10, where the signals of the donor and acceptor were detected, confirming its formation. The chemical shifts of the

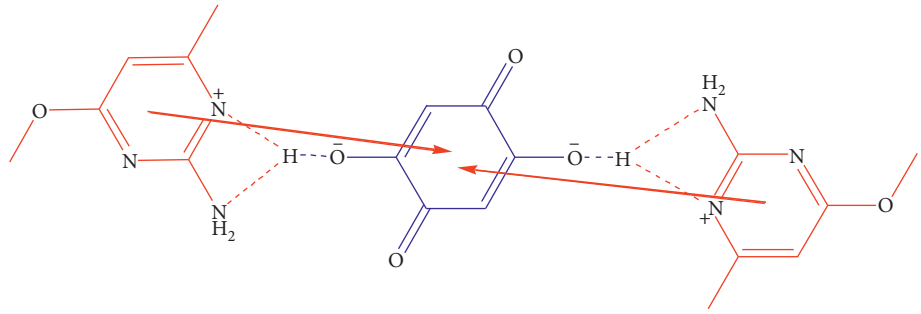

Scheme 3: The suggested molecular structure of the solid $[(AMMP)_2(DHBQ)]$ HB-CT complex.

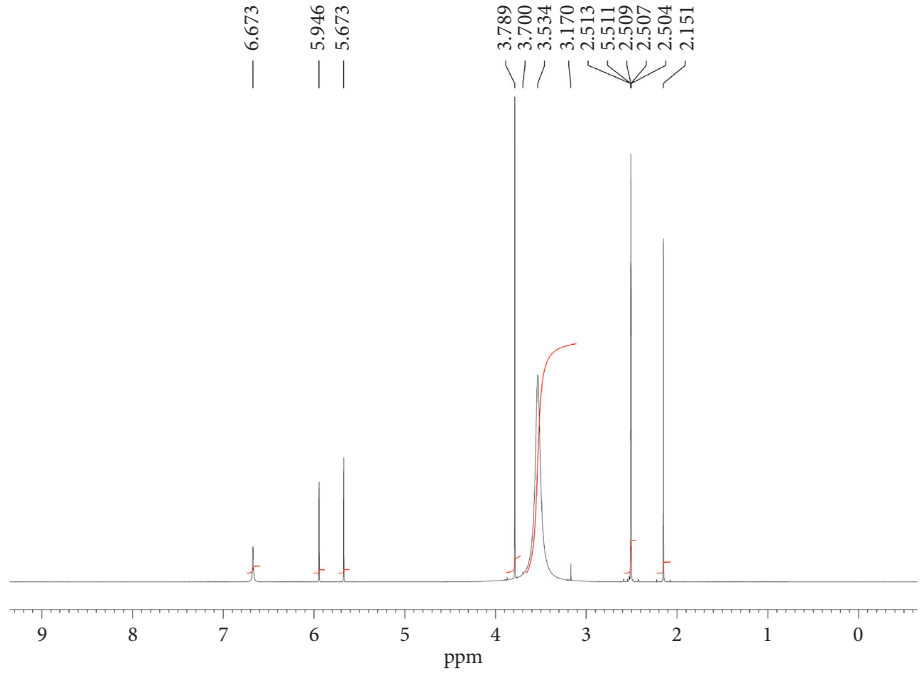

Figure 10: ^{1}H NMR spectrum of the solid $[(AMMP)_2(DHBQ)]$ complex in DMSO-d_6.

reactant molecules and the HB-CT complex are compiled in Table 6. Shifts in the resonance signals were recorded in the complex spectrum compared with that of the donor and acceptor molecules due to the change in the electronic structure upon complexation. For example, a singlet resonance signal of methyl group protons was shifted to $\delta = 2.151$ ppm compared with $\delta = 2.125$ ppm in the free AMMP. Also, the signal of methoxy group protons was shifted to $\delta = 3.789$ ppm compared with $\delta = 3.764$ ppm in the free AMMP. The singlet resonance signal of the two symmetrical protons of C_3 and C_6 of the DHBQ moiety was shifted to $\delta = 5.863$ ppm. Hence, the shifts in the resonance signal positions confirmed the charge transfer from the DHBQ to the AMMP. From Figure 10, the disappearance of the hydroxyl proton signal of DHBQ above $\delta = 7$ ppm is clearly observed, supporting the formation of hydrogen-bonded CT complex. Instead, a new broad signal centered at $\delta = 3.534$ ppm is identified, which is assigned to the hydrogen bond formed between the ring nitrogen and the hydroxyl proton of the DHBQ. Also, a downfield shift of the amino group protons signals to $\delta = 6.673$ ppm compared with $\delta = 6.460$ ppm for the amino protons in the free AMMP, which is due to the deshielding of the amino group protons as a result of the hydrogen bond formation (Scheme 3). Consequently, ^{1}H NMR results are in agreement with FTIR results.

Table 6: The chemical shifts δ (ppm) of the reactants and the HB-CT complex.

Assignment	DHBQ	AMMP	HB-CT complex
1H: OH	10.899	—	—
2H: $C_{(3,5)}H$	5.863	—	5.946
3H: $C_{(6)}CH_3$	—	2.125	2.151
3H: OCH_3	—	3.764	3.789
1H: $C_{(5)}H$	—	5.882	5.673
2H: NH_2	—	6.460	6.673
1H, hydrogen bonding: $^+N_{(1)}H$	—	—	b, 3.534

Table 7: Thermogravimetric data for the $[(AMMP)_2(DHBQ)]$ complex.

Complex	Stage	TG temperature range (°C)	DTG temperature peak (°C)	Mass loss (%) obs./ calc.	Lost species
$[(AMMP)_2(DHBQ)]$	I	135–275	194	94.75/94.27	$C_{16}H_{22}N_6O_6$ organic moiety
	Residue	>275	—	5.25/5.73	2C

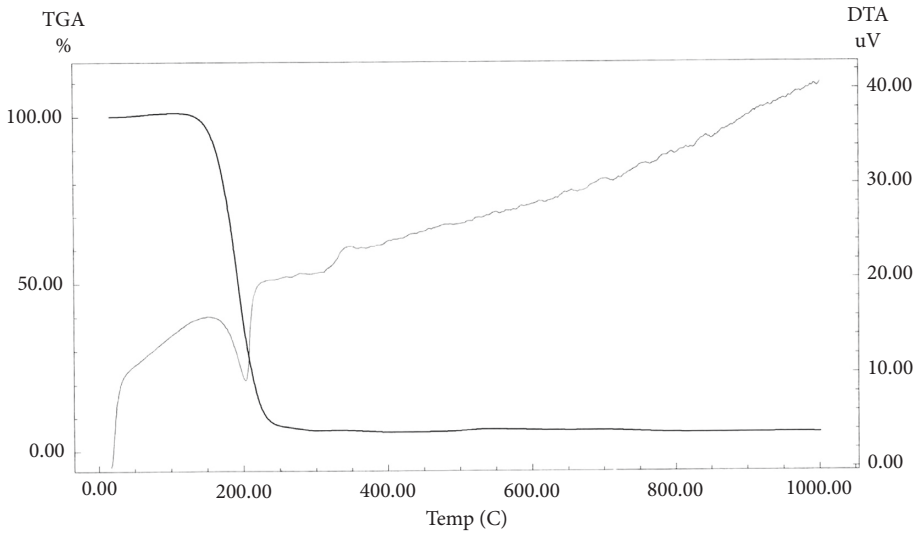

Figure 11: TGA/DTG thermal diagrams of the solid $[(AMMP)_2(DHBQ)]$ complex.

3.5.3. Thermal Analysis. TG and DTA are very useful for studying the decomposition and, thus, the stability of solid HB-CT complexes. In the present study, the TG-DTA measurements were performed under a nitrogen gas flow of 20 mL min^{-1} in the temperature range 10°C–1000°C at a heating rate of 10°C min^{-1}. The thermal data for the HB-CT complex are given in Table 7. The thermal behavior of the solid $[(AMMP)_2(DHBQ)]$ complex is shown in Figure 11, where only one strong peak is observed, indicating that the formed complex is a new organic compound that has one sharp melting point [52]. The complex shows endothermic decomposition at DTA max (140°C to 235°C) = 194°C, which corresponds to the loss of the organic moiety $C_{16}H_{22}N_6O_6$ with an observed weight loss of 94.75% (calc. = 94.27%).

3.5.4. Powder XRD Analysis. The structure and particle size of the synthesized $[(AMMP)_2(DHBQ)]$ HB-CT complex were investigated by XRD analysis. Figure 12 shows the XRD pattern of the complex in the range $0 < 2\theta < 120°$. A sharp and strong characteristic Bragg peak is observed at $2\theta = 30.91°$. The appearance of sharp and well-defined Bragg peaks at specific 2θ angles confirms the semicrystalline structure of the $[(AMMP)_2(DHBQ)]$ complex. Based on the highest intensity value and XRD data, the particle size of the complex was calculated using the Debye–Scherrer equation [53]:

$$D = \frac{0.94\lambda}{\beta \cos\theta}, \quad (9)$$

where D is the apparent particle size of the grains in nm, 0.94 is the Scherrer constant, λ is the wavelength of the incident X-rays (Co K_α: 1.7890 Å), θ is the position of the selected diffraction peak, and β is the full-width at half-maximum (FWHM) of the characteristic XRD peaks in radians. The values of the Bragg angle (2θ), β of the main intensity peak, the interplanar spacing between atoms (d), the relative intensity, and the calculated particle size (D) in nm are shown in Table 8. The calculated particle size of the $[(AMMP)_2(DHBQ)]$ complex was found to be ca. 23 nm, which demonstrates that the complex particles are in the nanoscale range.

3.6. Antimicrobial Activity Studies. Both the donor (AMMP) and its synthesized HB-CT complex were tested *in vitro* for antimicrobial activity against several microbes including Gram-positive bacteria, Gram-negative bacteria, and fungi. The microorganisms used in this study are commonly applied in research into new antimicrobial agents [54].

We first performed a preliminary screening by the well diffusion method to assess AMMP and the new HB-CT complex for antimicrobial properties. The $[(AMMP)_2(DHBQ)]$ complex was found to exhibit antimicrobial activity, as shown in Table 9. The results given in Table 9 indicate that the new complex has high inhibitory activities against Gram-negative and Gram-positive bacteria, as revealed by the diameters of their inhibition zones (˃10 mm). Also, the activity of the HB-CT complex is comparable with that of neomycin for Gram-negative and Gram-positive bacteria. Overall, the results demonstrate that the new HB-CT complex synthesized in this study exhibits strong

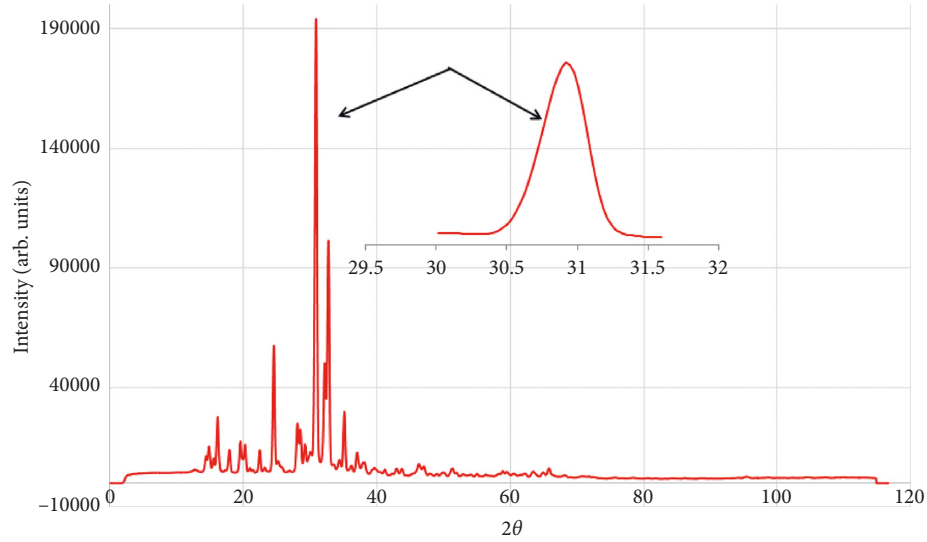

Figure 12: XRD pattern for the $[(AMMP)_2(DHBQ)]$ HB-CT complex.

Table 8: XRD data for the $[(AMMP)_2(DHBQ)]$ complex.

Complex	2θ (°)	d value (A)	FWHM	Relative intensity (%)	Particle size (nm)
$[(AMMP)_2(DHBQ)]$	30.91	3.357	0.3263	100	23

Table 9: Antimicrobial activity of the $[(AMMP)_2(DHBQ)]$ complex at the concentration of 100 $\mu g \cdot mL^{-1}$.

	Diameter of inhibition zone (mm)		
	Donor	CT complex	Neomycin
Bacteria			
Bacillus subtilis	16	20	24
Staphylococcus aureus	18	22	18
Sarcina lutea S.	16	18	20
Escherichia coli	18	24	22
Pseudomonas aeruginosa	16	20	20
Klebsiella pneumonia	16	18	14
	Donor	CT complex	Tetracycline
Fungi			
Candida albicans	14	20	18
Aspergillus niger	16	18	14
Penicillin sp.	16	20	22

antibacterial activities with significant zones of inhibition (≥20 mm) against all the tested bacteria.

The $[(AMMP)_2(DHBQ)]$ HB-CT complex is of special interest since it shows inhibition of all tested fungi, whereas the tetracycline control failed to affect the growth of *Aspergillus niger*. Furthermore, the complex presented an inhibition zone for certain bacterial strains equivalent to that for 30 mg of tetracycline. The high antimicrobial activity of the $[(AMMP)_2(DHBQ)]$ complex can be attributed to the presence of both pyrimidine and *p*-benzoquinone rings, which are known for their biological activities [55, 56]. Furthermore, it has been reported in the literature that heterocyclic compounds with electron-donating methoxy group substituents at the *para* position of the aromatic rings exhibit excellent antimicrobial activity [57–59].

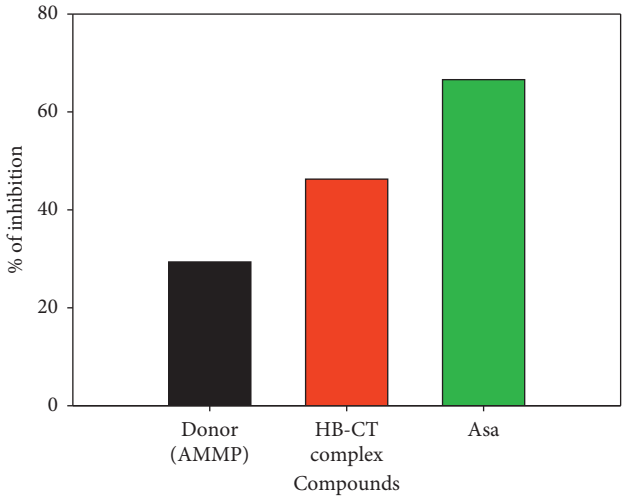

Figure 13: Antioxidant activity of the solid $[(AMMP)_2(DHBQ)]$ complex.

3.7. Antioxidant Activity. The DPPH radical scavenging activity of the $[(AMMP)_2(DHBQ)]$ complex was assessed using Asa as standard for comparison. The HB-CT complex shows good capacity for DPPH scavenging, as shown in Figure 13, which indicates that it exhibits antioxidant activity.

4. Conclusions

The HB-CT interactions between AMMP as an electron donor and DHBQ as a π-acceptor were studied in MeOH using UV-Vis spectroscopy, whereas the solid HB-CT complex was characterized by CHN, FTIR, ^{1}H NMR, XRD, and TG/DTA analyses, revealing that AMMP is found to form a stable 1 : 1 HB-CT complex with DHBQ in MeOH and a stable 2 : 1 [$(AMMP)_2$(DHBQ)] complex as a solid. The high stabilities of the complex in both states are due to the fact that AMMP is a good donor and DHBQ is a good acceptor, leading to strong hydrogen bonding in the formed complex. Furthermore, the MeOH plays a twofold role as both hydrogen bond donor and hydrogen bond acceptor, which is assumed to increase the stability of the HB-CT complex. XRD analysis revealed that the synthesized complex has a nanocrystalline structure with a particle diameter of ca. 23 nm.

Furthermore, the antimicrobial and antioxidant activities of the HB-CT complex were studied. *In vitro* antimicrobial evaluation revealed that the complex exhibits inhibitory activities against a wide range of microorganisms comparable (and in certain cases superior) to those of tetracycline and neomycin. Furthermore, the complex was demonstrated to exhibit antioxidant activity against DPPH radicals. Thus, the prepared complex has enormous promise as antimicrobial agent. However, more work is required to evaluate the cytotoxicity of the complex, particularly toward eukaryote cells. Thus, cytotoxicity tests are an absolute necessity if the synthetic complex is to be utilized as a pharmaceutical.

Data Availability

The electronic absorbance, calculations, and the biological experiment data used to support the findings of this study are available from the corresponding author upon request (rmalghanmi@uj.edu.sa).

Conflicts of Interest

The authors declare that they have no conflicts of interest.

References

[1] A. S. Gaballa and A. S. Amin, "Preparation, spectroscopic and antibacterial studies on charge-transfer complexes of 2-hydroxypyridine with picric acid and 7,7′,8,8′-tetracyano- p -quinodimethane," *Spectrochimica Acta Part A: Molecular and Biomolecular Spectroscopy*, vol. 145, pp. 302–312, 2015.

[2] G. Vadivelan, M. Saravanabhavan, V. Murugesan, and M. Sekar, "Synthesis, characterization and biological studies of a charge transfer complex: 2-aminopyridinium-4-methylbenzenesulfonate," *Spectrochimica Acta Part A: Molecular and Biomolecular Spectroscopy*, vol. 145, pp. 461–466, 2015.

[3] J. Quiroga, P. E. Romo, A. Ortiz et al., "Synthesis, structures, electrochemical studies and antioxidant activity of 5-aryl-4-oxo-3,4,5,8-tetrahydropyrido[2,3-d]pyrimidine-7-carboxylic acids," *Journal of Molecular Structure*, vol. 1120, pp. 294–301, 2016.

[4] A. M. Slifkin, *Charge Transfer Interaction of Biomolecules*, New York: Academic Press, New York, NY, USA, 1971.

[5] H. Salem, "Spectrophotometric determination of β-adrenergic blocking agents in pharmaceutical formulations," *Journal of Pharmaceutical and Biomedical Analysis*, vol. 29, no. 3, pp. 527–538, 2002.

[6] V. Murugesan, M. Saravanabhavan, and M. Sekar, "Synthesis, spectroscopic characterization and structural investigation of a new charge transfer complex of 2,6-diaminopyridine with 4-nitrophenylacetic acid: antimicrobial, DNA binding/cleavage and antioxidant studies," *Spectrochimica Acta Part A: Molecular and Biomolecular Spectroscopy*, vol. 147, pp. 99–106, 2015.

[7] S. M. Andrade, S. M. B. Costa, and R. Pansu, "Structural changes in W/O TRITON X-100/cyclohexane-hexanol/water microemulsions probed by a fluorescent drug *Piroxicam*," *Journal of Colloid and Interface Science*, vol. 226, no. 2, pp. 260–268, 2000.

[8] K. Takahasi, K. Horino, T. Komura, and K. Murata, "Photovoltaic properties of porphyrin thin films mixed with o-chloranil," *Bulletin of the Chemical Society of Japan*, vol. 66, no. 3, pp. 733–738, 1993.

[9] A. Eychmüller and A. L. Rogach, "Chemistry and photophysics of thiol-stabilized II-VI semiconductor nanocrystals," *Pure and Applied Chemistry*, vol. 72, no. 1-2, pp. 179–188, 2000.

[10] X. L. Duan, D. R. Yuan, X. Q. Wang et al., "Preparation and characterization of nonlinear optical crystal materials: cadmium mercury thiocyanate and its Lewis base adducts," *Crystal Research and Technology*, vol. 37, no. 5, pp. 446–455, 2002.

[11] T. S. Belal, D. S. El-Kafrawy, M. S. Mahrous, M. M. Abdel-Khalek, and A. H. Abo-Gharam, "Validated spectrophotometric methods for determination of sodium valproate based on charge transfer complexation reactions," *Spectrochimica Acta Part A: Molecular and Biomolecular Spectroscopy*, vol. 155, pp. 47–53, 2016.

[12] A. A. Gouda and M. Kasssem, "Novel spectrophotometric methods for determination of desloratidine in pharmaceutical formulations based on charge transfer reaction," *Arabian Journal of Chemistry*, vol. 9, pp. s1712–s1720, 2016.

[13] M. E. Mohamed, E. Y. Z. Frag, A. A. Hathoot, and E. A. Shalaby, "Spectrophotometric determination of fenoprofen calcium drug in pure and pharmaceutical preparations. Spectroscopic characterization of the charge transfer solid complexes," *Spectrochimica Acta Part A: Molecular and Biomolecular Spectroscopy*, vol. 189, pp. 357–365, 2018.

[14] H. H. Eldaroti, S. A. Gadir, M. S. Refat, and A. M. A. Adam, "Charge-transfer interaction of drug quinidine with quinol, picric acid and DDQ: spectroscopic characterization and biological activity studies towards understanding the drug-receptor mechanism," *Journal of Pharmaceutical Analysis*, vol. 4, no. 2, pp. 81–95, 2014.

[15] T. P. Selvam, C. R. James, P. V. Dniandev, and S. K. Valzita, "A mini review of pyrimidine and fused pyrimidine marketed drugs," *Research in Pharmacy*, vol. 2, no. 4, pp. 01–09, 2012.

[16] M. Asif, "The pharmacological importance of some diazine containing drug molecules," *SOP Transactions on Organic Chemistry*, vol. 1, no. 1, pp. 1–10, 2014.

[17] S. Lahmidi, E. H. Anouar, M. El Hafi et al., "Synthesis, X-ray, spectroscopic characterization, DFT and antioxidant activity of 1,2,4-triazolo[1,5-a]pyrimidine derivatives," *Journal of Molecular Structure*, vol. 1177, pp. 131–142, 2019.

[18] I. M. Lagoja, "Pyrimidine as constituent of natural biologically active compounds," *Chemistry & Biodiversity*, vol. 2, no. 1, pp. 1–50, 2005.

[19] J. I. Segal and B. S. Brunnemann, "4-Aminopyridine improves pulmonary function in quadriplegic humans with Long-standing spinal cord injury," *Pharmacotherapy*, vol. 17, no. 3, pp. 415–423, 1997.

[20] A.-G. E. Amr, A. M. Mohamed, S. F. Mohamed, N. A. Abdel-Hafez, and A. E.-F. G. Hammam, "Anticancer activities of some newly synthesized pyridine, pyrane, and pyrimidine derivatives," *Bioorganic & Medicinal Chemistry*, vol. 14, no. 16, pp. 5481–5488, 2006.

[21] I. O. Zhuravel, S. M. Kovalenko, A. V. Ivachtchenko, K. V. Balakin, and V. Kazmirchuk, "Synthesis and antimicrobial activity of 5-hydroxymethyl- 8-methyl-2-(*N*-arylimino)-pyrano[2,3-c]pyridine-3-(*N*-aryl)-carboxamides," *Bioorganic Medicinal Chemistry Letters*, vol. 15, no. 24, pp. 5483–5487, 2005.

[22] H. G. Sogukomerogullari, T. T. Tok, F. Yilmazi, I. Berber, and M. Sonmez, "Synthesis, characterization, biological studies, and molecular modeling of mixed ligand bivalent metal complexes of Schiff bases based on *N*-aminopyrimidine-2-one/2-thione," *Turkish Journal of Chemistry*, vol. 39, pp. 497–509, 2015.

[23] M. Hafeez and M. Riaz, "Aminopyridine stabilized group-IV metal complexes and their applications," *Applied Petrochemical Research*, vol. 6, no. 4, pp. 307–340, 2016.

[24] A. Sobola, G. Watkins, and B. van, "Synthesis, characterization and biological study of Cu(II) complexes of aminopyridine and (aminomethyl)pyridine Schiff bases," *Journal of the Serbian Chemical Society*, vol. 83, no. 7-8, pp. 809–819, 2018.

[25] M. M. Habeeb, A. S. AL-Attas, and M. T. Basha, "Spectrophotometric studies of proton transfer complexes between 2-amino-4-methoxy-6-methyl-pyrimidine and 2-amino-4,6-dimethyl-pyrimidine with 2,6-dichloro-4-nitrophenol in acetonitrile," *Journal of Molecular Liquids*, vol. 150, no. 1–3, pp. 56–61, 2009.

[26] A. S. AL-Attas, M. M. Habeeb, and D. S. AL-Raimi, "Synthesis and spectroscopic studies of charge transfer complexes between chloranilic acid and some heterocyclic amines in ethanol," *Journal of Molecular Structure*, vol. 928, no. 1–3, pp. 158–170, 2009.

[27] R. M. Alghanmi, "Spectrophotometric study of charge transfer complex between 2,6-diaminopyridine and 2,5-dihydroxy-p-benzoquinone," *Physics and Chemistry of Liquids*, vol. 51, no. 3, pp. 365–380, 2013.

[28] R. M. Alghanmi, "Solvation and temperature effect on the charge-transfer complex between 2-amino-4-picoline with 2,5-dihydroxy-p-benzoquinone," *Physics and Chemistry of Liquids*, vol. 51, no. 5, pp. 635–650, 2013.

[29] R. M. Alghanmi and M. M. Habeeb, "Spectral and solvation effect studies on charge transfer complex of 2, 6-diaminopyridine with chloranilic acid," *Journal of Molecular Liquids*, vol. 181, pp. 20–28, 2013.

[30] R. M. Alghanmi and M. M. Habeeb, "Spectroscopic, thermal studies and molecular modelling of charge transfer complexation between 5-amino-2-methoxypyridine with chloranilic acid in different polar solvents," *Physics and Chemistry of Liquids*, vol. 53, no. 4, pp. 490–505, 2015.

[31] I. Ahmad and A. Z. Beg, "Antimicrobial and phytochemical studies on 45 Indian medicinal plants against multi-drug resistant human pathogens," *Journal of Ethnopharmacology*, vol. 74, no. 2, pp. 113–123, 2001.

[32] A. H. Collins, *Microbiology Method*, Butterworth, Oxford, UK, 2nd edition, 1976.

[33] R. Cruickshank, J. P. Duguid, B. P. Marmion, and R. H. A. Awain, *Medicinal Microbiology*, Churchill Livinggstone, London, UK, 12th edition, 1995.

[34] M. Mekni, R. Azez, M. Tekaya, B. Mechri, and M. Hammami, "Phenolic non-phenolic compounds and antioxidant activity of pomegranate flower, leaf and bark extracts of four Tunisian cultivars," *Journal of Medicinal Plants Research*, vol. 7, no. 17, pp. 1100–1107, 2013.

[35] P. Jop, "Formation and stability of inorganic complexes in solution," *Annali di Chimica et de Physique*, vol. 9, pp. 113–203, 1928.

[36] H. A. Benesi and J. H. Hildebrand, "A spectrophotometric investigation of the interaction of iodine with aromatic hydrocarbons," *Journal of the American Chemical Society*, vol. 71, no. 8, pp. 2703–2707, 1949.

[37] A. Airini, M. Homocianu, and D. O. Dorohoi, "Changes induced by solvent polarity in electronic absorption spectra of some azo disperse dyes," *Journal of Molecular Liquids*, vol. 157, no. 1, pp. 13–17, 2010.

[38] R. M. Alghanmi, S. M. Soliman, M. T. Basha, and M. M. Habeeb, "Electronic spectral studies and DFT computational analysis of hydrogen bonded charge transfer complexes between chloranilic acid and 2,5-dihydroxy-p-benzoquinone with 2-amino-4-methylbenzothiazole in methanol," *Journal of Molecular Liquids*, vol. 256, pp. 433–444, 2018.

[39] G. G. Aloisi and S. Pignataro, "Molecular complexes of substituted thiophens with σ and π acceptors. Charge transfer spectra and ionization potentials of the donors," *Journal of the Chemical Society, Faraday Transactions 1: Physical Chemistry in Condensed Phases*, vol. 69, pp. 534–539, 1973.

[40] A. B. P. Leve, *Inorganic Electronic Spectroscopy*, Elsevier, Amsterdam, Netherlands, 2nd edition, 1985.

[41] E. M. Voigt and C. Reid, "Ionization potentials of substituted benzenes and their charge-transfer spectra with tetracyanoethylene," *Journal of the American Chemical Society*, vol. 86, no. 19, pp. 3930–3934, 1964.

[42] R. Rathore, S. V. Lindeman, and J. K. Kochi, "Charge-transfer probes for molecular recognition via steric hindrance in donor-acceptor pairs," *Journal Of the American Chemical Society*, vol. 119, no. 40, pp. 9393–9404, 1997.

[43] G. Briegleb, "Elektronen affinitäten organischer Moleküle," *Angewandte Chemie*, vol. 76, no. 8, pp. 326–341, 1964.

[44] G. Briegleb and J. Czekalla, "The intensity of electron transition bands in electron donator-acceptor complexes," *Zeitschrift für Physikalische Chemie*, vol. 24, no. 1-2, pp. 37–54, 1960.

[45] M. Pandeeswaran and K. P. Elango, "Solvent effect on the charge transfer complex of oxatomide with 2,3-dichloro-5,6-dicyanobenzoquinone," *Spectrochimica Acta Part A: Molecular and Biomolecular Spectroscopy*, vol. 65, no. 5, pp. 1148–1153, 2006.

[46] G. N. Lewis and M. Randall, *Thermodynamics*, McGraw-Hill, New York, NY, USA, 2nd edition, 1961.

[47] P. D. Ross and S. Subramanian, "Thermodynamics of protein association reactions: forces contributing to stability," *Biochemistry*, vol. 20, no. 11, pp. 3096–3102, 1981.

[48] W. B. Person, "Thermodynamic properties of donor-acceptor complexes," *Journal of the American Chemical Society*, vol. 84, no. 4, pp. 536–540, 1962.

[49] N. Singh and A. Ahmad, "Spectrophotometric and spectroscopic studies of charge transfer complex of 1-naphthylamine

as an electron donor with picric acid as an electron acceptor in different polar solvents," *Journal Of Molecular Structure*, vol. 977, no. 1–3, pp. 197–202, 2010.

[50] J. C. Miller and N. A. Miller, *Statistics for Analytical Chemistry*, Ellis Horwood Ltd., Chichester, UK, 2nd edition, 1988.

[51] H. M. N. H. Irving, H. Freiser, and T. S. West, *IUPAC Compendium of Analytical Nomenclature Definitive Rules*, Pergamum Press, Oxford, UK, 1981.

[52] M. S. Refat, L. A. El-Zayat, and O. Z. Yeşilel, "Synthesis and spectroscopic characterization of piperidine/chloranil and piperidine/7,7′,8,8′-tetracyanoquinodimethane charge transfer complexes: X-ray crystal structure of a 7,7-dicyano-8,8-di-piperidinoquinodimethane adduct," *Polyhedron*, vol. 27, no. 2, pp. 475–484, 2008.

[53] M. A. Estermann, W. I. F. David, K. Shankland, L. B. Mccusker, and C. Baerlocher, *Structure Determination from Powder Diffraction Data (SDPD)*, Oxford Science Publications, New York, NY, USA, 2002.

[54] V. Murugesan, M. Saravanabhavan, and M. Sekar, "Synthesis, characterization and pharmacological investigation of a new charge-transfer complex of 3-aminopyridinum-p-toluene-sulfonate," *Journal of Molecular Structure*, vol. 1084, pp. 95–102, 2015.

[55] V. Sharma, N. Chitranshi, and A. K. Agarwal, "Significance and biological importance of pyrimidine in the microbial World," *International Journal of Medicinal Chemistry*, vol. 2014, Article ID 202784, 31 pages, 2014.

[56] A. F. Tuyun and M. Yıldız, "Synthesis and characterization of new cyclic aminobenzoquinones," *Journal of the Turkish Chemical Society, Section A: Chemistry*, vol. 5, no. 2, pp. 371–380, 2018.

[57] M. Gopalakrishnan, J. Thanusu, and V. Kanagarajan, "Design, synthesis, spectral analysis andin vitromicrobiological evaluation of 2-phenyl-3-(4,6-diarylpyrimidin-2-yl)thiazolidin-4-ones," *Journal of Enzyme Inhibition and Medicinal Chemistry*, vol. 24, no. 5, pp. 1088–1094, 2009.

[58] Y. Narain, S. Jhaumeer-Laulloo, and M. G. Bhowon, "Structure-activity relationship of Schiff base derivatives of bis(aminophenyl)disulfide and p-vanillin as antimicrobial agents," *International Journal of Biological and Chemical Science*, vol. 4, no. 1, pp. 69–74, 2010.

[59] M. Malhotra, P. Hans, S. Sharma, A. Deep, and P. Phogat, "Synthesis and characterization of (Z)-N-(1-[2-{3-[(dimethylamino)methyl)]- 2-methoxyphenyl}-5-(pyridin-4-YL)-1,3,4-oxadiazol-3(2H)-YL]ethylidene) benzenamine derivatives as potent antifungal agents," *Acta Poloniae Pharmaceutica–Drug Research*, vol. 69, no. 3, pp. 433–438, 2012.